Equations of State of Matter at High Energy Densities

V.E. Fortov and I.V. Lomonosov[*]

Institute of Problems of Chemical Physics RAS, Prosp. Akad. Semenova, 1, Chernogolovka 142432, Moscow Reg., Russia

Abstract: The physical properties of hot dense matter over a broad domain of the phase diagram are of interest in astrophysics, planetary physics, power engineering, controlled thermonuclear fusion, impulse technologies, enginery, and other applications. The present report reviews the contribution of modern experimental methods and theories to the problem of the equation of state (EOS) at extreme conditions. Experimental techniques for high pressures and high energy density cumulation, the drivers of intense shock waves, and methods for the fast diagnostics of high-energy matter are considered. It is pointed out that the available high pressure and temperature information covers a broad range of the phase diagram, but only irregularly and, as a rule, is not thermodynamically complete; its generalization can be done only in the form of a thermodynamically complete EOS. As a practical example, construction of multi-phase EOS for tungsten is presented. The model's results are shown for numerous shock-wave data, the high-pressure melting and evaporation regions and the critical point of tungsten.

Keywords: Shock waves, equation of state, tungsten.

1. INTRODUCTION

Equation of state (EOS) describes fundamental thermophysical properties of matter. This information can only be obtained by using sophisticated theoretical models or from experiments [1-5]. The EOS is of considerable interest for basic research and has numerous important applications [6-8]. States of matter characterized by high-energy-density occupy a broad region of the phase diagram, for example, hot compressed matter, strongly coupled plasmas, hot expanded liquid and quasi-ideal plasmas. Our knowledge of these states is limited, because theoretical modeling is complicated and experiments are difficult to perform.

In this paper, we present a review of current state of art of investigations at high pressures, high temperatures. It includes results of static and dynamic experiments and modern theories and their possibilities and role in understanding of materials properties in a wide range of the phase diagram.

Finally, an example of construction of multi-phase EOS for tungsten is presented. The EOS provides for a correct description of phase boundaries, melting and evaporation, as well as the effects of the first and second ionization. To construct the EOS, the following information was used at high pressure and high temperature: measurements of isothermal compressibility in diamond anvil cells, isobaric-expansion measurements, data on the shock compressibility of solid and porous samples, impedance measurements of shock compressibility obtained by an underground nuclear explosion, data on the isentropic expansion of shocked metals, calculations by the Thomas-Fermi model, numerous evaluations of the critical point.

*Address correspondence to this author at the Institute of Problems of Chemical Physics RAS, Prosp. Akad. Semenova, 1, Chernogolovka 142432, Moscow Reg., Russia; Tel: +007 (496) 5249472; Fax: +007 (496) 5249472; E-mail: ivl143@yahoo.com

2. EOS PROBLEM

The equation of state (EOS) is a fundamental property of matter defining its thermodynamic characteristics in a functional form like $f(x, y, z) = 0$, where x, y, z can be, for example, volume V, pressure P, temperature T, or in the form of graphs or tables. Well known functional for EOSs include, for instance, the Mie-Grüneisen EOS [9]

$$P(V, E) = P_c(V) + \frac{\gamma(V)}{V}(E - E_c(V)), \tag{1}$$

where the index c indicates the component at $T = 0$ K; the Birch potential [10]

$$P(V) = \frac{3}{2} B_T (\sigma^{7/3} - \sigma^{5/3})\{1 - \frac{3}{4}(4 - B_P)(\sigma^{2/3} - 1)\}, \tag{2}$$

in which $\sigma = V_0 / V$, V_0-specific volume at normal conditions ($P = 1$ bar, $T = 298$ K), $B_T = -(\partial P / \partial \ln V)_T$-isothermal bulk compression modulus, $B_P = \partial B_T / \partial P$-its pressure derivative; and the Carnahan-Starling's approximation for the free energy of a system of "hard" spheres [11]

$$\frac{F_{HS}(V, T)}{NkT} = \frac{4\eta - 3\eta^2}{(1 - \eta)^2}, \tag{3}$$

where N-amount of particles, k-Boltzmann's constant and η-packing density. One can find examples of EOSs in graphic or tabular form in compendia of shock wave data [12-15]; these are EOSs of shock adiabats.

Nowadays EOS means material's properties at high energy density (HED). The state of matter at extremely high temperatures and densities, and hence with extraordinarily high energy densities, has always attracted researchers due to the possibility of reaching new parameter records, the prospect of advancing to new regions of the phase diagram,

and the potentiality of producing in laboratory conditions the exotic states that gave birth to our Universe through the Big Bang and account for wherein the great bulk (95%) of baryon (visible) matter in nature now resides: in the plasmas of ordinary and neutron stars, pulsars, black holes, and giant planets, as well as in the multitude of planets, including those discovered quite recently.

A stable pragmatic incentive to pursue suchlike investigations is the practical application of extreme states in nuclear, thermonuclear, and pulsed energetics, as well as in high-voltage and high-power electrophysics, and for the synthesis of superhard materials, for strengthening and welding materials, for the impact protection of space vehicles, and, of course, in the field of defense - because the operation of nuclear devices with controllable (inertial controlled thermonuclear fusion, ICTF) and quasicontrollable (atomic and hydrogen bombs) energy release relies on the initiation of nuclear reactions in a strongly compressed and heated nuclear fuel.

The development of the physics of extremely high energy densities is largely determined by the implementation of defense, space, and nuclear programs in which extremely high pressures and temperatures are the elements required for directional action on substances and the initiation of nuclear reactions in compressed and heated nuclear fuel. At the same time, the range of technical applications related to the physics of extreme states is broadening constantly. These states of matter underlie the operation of pulsed thermonuclear reactors with the inertial confiment of hot plasma, high-power magnetohydrodynamic and explosive magnetic generators, power installations and rocket propulsors with gas-phase nuclear reactors, plasmachemical and microwave reactors, plasmatrons, and high-power sources of optical and X-ray radiation. Extreme states emerge when a substance is subjected to intense shock, detonation, and electroexplosion waves, concentrated laser radiation, and electron and ion beams, as well as in powerful chemical and nuclear explosions, in the pulsed vaporization of liners in pinches and magnetic cumulation generators, in the hypersonic motion of bodies in dense planetary atmospheres, in high-velocity impacts, and in many other situations characterized by ultimately high pressures and temperatures. The physics of near-electrode, contact, and electroexplosion processes in a vacuum breakdown is intimately related to the high-energy plasma which determines the operation of high-power pulsed accelerators, microwave radiation generators, and plasma switches. This list can easily be extended.

High energy density physics has been making rapid strides due to the advent of new devices for the generation of high energy densities, like relativistic ion accelerators, lasers, high-current Z-pinches, explosive and electroexplosion generators of intense shock waves, multistage light-gas guns, and diamond anvils. These complex and expensive technical devices have made it possible to substantially advance along the scale of energy density attainable in a physical experiment and to obtain in laboratory or quasilaboratory conditions the macroscopic volumes of matter in states that range into the megabar-gigabar pressure domain unattainable with the traditional techniques of experimental physics.

We see, that HED physics deals with EOS of matter in very broad range of the phase diagram: from compressed solid to hot liquid and non-ideal plasma, characterized by extremely high pressure and temperature.

3. EOS: THEORY AND EXPERIMENT

The current state of the problem of a theoretical description of thermodynamic properties of matter at high pressures and high temperatures is given in a set of publications (see refs. [2-4, 7, 8, 16] and references therein). In spite of the significant progress achieved in predicting EOS information accurately in solid, liquid, and plasma states with the use of the most sophisticated "ab initio" computational approaches (classic and quantum methods of self-consisted field, diagram technique, Monte-Carlo, and molecular dynamics methods), the disadvantage of these theories is their regional character [2-4, 7, 8]. For example, the Schrodinger equation is solving for crystal at $T = 0$ K [17], while integral equations relate pair interactive potential and pair correlation function for liquid [18] and chemical potentials are used in the "chemical" model of plasmas [8].

The range of applicability of each method is local and, rigorously speaking, no single one of them provides for a correct theoretical calculation of thermodynamic properties of matter on the whole phase plane from the cold crystal to the liquid and hot plasmas [2, 3, 8]. The principal problem here is the need to account correctly for the strong collective interparticle interaction in disordered media, which presents special difficulties in the region occupied by dense, disordered, nonideal plasmas [2-4, 7, 8].

In this case, experimental data at high pressures and high temperatures are of particular significance, because they serve as reference points for theories and semi-empirical models. Data obtained with the use of dynamic methods (see [1, 7, 8, 16, 19-21] and references therein) are of the importance from the practical point of view. Shock-wave methods permit to study a broad range of the phase diagram from the compressed hot condensed states to dense strongly coupled plasma and quasi-gas states. Detailed presentations of shock-wave methods to investigate high dynamic pressures is given in monographs [7, 8, 16, 20] and reviews [1, 21-23].

The available experimental information is shown in Fig. (**2**) on a 3D, relative volume-temperature-pressure surface for aluminum, calculated by a semi-empirical multi-phase EOS [24, 25]. The experimental data on the shock compression of solid and porous metals, as well as isentropic expansion, covers nine orders of magnitude in pressure and four in density. In a viscous compression shock termed the shock front, the kinetic energy of the oncoming flow is converted to the thermal energy of the compressed and irreversibly heated medium. This way of shock compression, see the principal Hugoniot in Fig. (**2**), has no limitations in the magnitude of the pressure obtained but is bounded by the short lifetimes of the shock-compressed substance. That is why the techniques employed for the diagnostics of these states should possess a high ($\sim 10^{-6} - 10^{-9}$ s) temporal resolution. When a stationary shock-wave discontinuity propagates through a material, the conservation laws of mass, momentum, and energy [16] are obeyed at its front.

These laws relate the kinematic parameters, the shock wave velocity D and the mass material velocity U behind the shock front, with thermodynamic quantities - the specific internal energy E, the pressure P, and the specific volume V:

$$\frac{V_0}{V} = \frac{D}{D-U}, \quad P = P_0 + \frac{DU}{V_0}, \quad E = E_0 + \frac{1}{2}(P+P_0)(V_0 - V). \quad (4)$$

Here the subscript 0 indicates the parameters of the immobile material ahead of the shock front. These equations permit determining the hydro- and thermodynamic characteristics of a shock-compressed mate rial upon recording any two of the five parameters E, P, V, D, and U, which characterize the shock discontinuity. Determined most easily and precisely by standard techniques is the shock velocity D. The choice of the second recorded parameter depends on specific experimental conditions. The "arrest" and "reflection" (impedance-matching) methods are using [1, 16] for condensed materials. Depending on experimental setup, either shock front velocities in target and etalon materials or the shock front velocity in target and the impactor velocity are measuring. Today, a wide variety of ways of generating intense shock waves is employed in dynamic experiments. These are chemical, nuclear, and electric explosions; pneumatic, gun powder, and electrodynamic guns; concentrated laser and soft X-ray radiation; and relativistic electron and ion beams [1, 8, 22, 26-31].

The first published shock-wave data were obtained for metals in the megabar (1 Mbar = 100 GPa) [32] and multimegabar [33, 34] pressure range using explosive drivers. Higher pressures of tens megabars have been accessed by spherical cumulative systems [35, 36] and by underground nuclear explosions [37, 38]. Maximum pressures of 400 TPa [39] were also reported for aluminum through the use of nuclear explosion. Note, that data obtained by impedance-matching techniques require the knowledge of the EOS for a standard material. Previously a monotonic approximation of the shock adiabat of lead between the traditional region of pressures $\leq$ 10 Mbar to Thomas-Fermi calculations [40] was used for the standard [37, 38]. It seems that iron, for which absolute Hugoniot measurements have been reported to pressures of 100 Mbar [41, 42], is now the best etalon material. Fig. (**1**) shows modern progress achieved in measurements of absolute shock compressibility with the use of traditional explosive techniques and investigations of impedance in experiments with concentrated energy fluxes like lasers and underground nuclear explosions.

The extension of the phase diagram data to greater relative volumes, in comparison with the principal Hugoniot, is achieved with shock compression of porous samples [16]. Nevertheless, difficulties in fabricating highly porous targets and non-uniform material response of the porous sample to shock loading imposes a practical limit to the minimum density of a specimen. The method of isentropic expansion of shocked matter, depending on the magnitude of the shock pressure and, consequently, the entropy provided, produces in one experiment transitions from a hot metallic liquid

shocked state, to a strongly coupled plasma, then to a two-phase liquid-gas region, and to a Boltzmann's weakly ionized plasma, and finally to a nearly ideal gas [7, 8, 16].
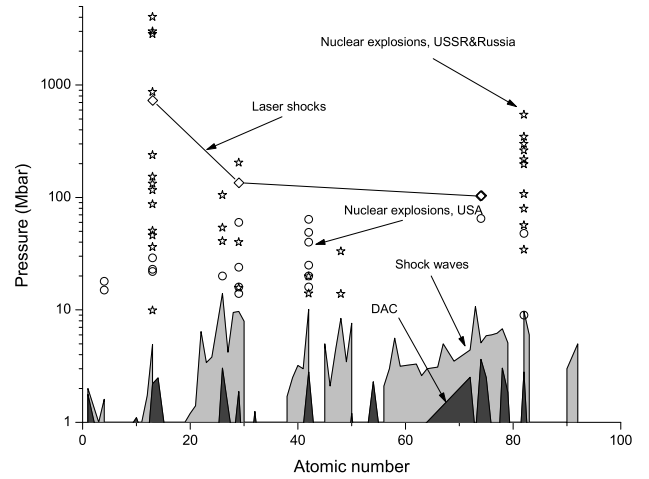
Fig. (1). The investigated pressure scale for the elements. Shown are maximum pressures achieved using traditional explosive (gray region), lasers, diamond-anvil-cell static measurements (black), and underground nuclear explosions (points).
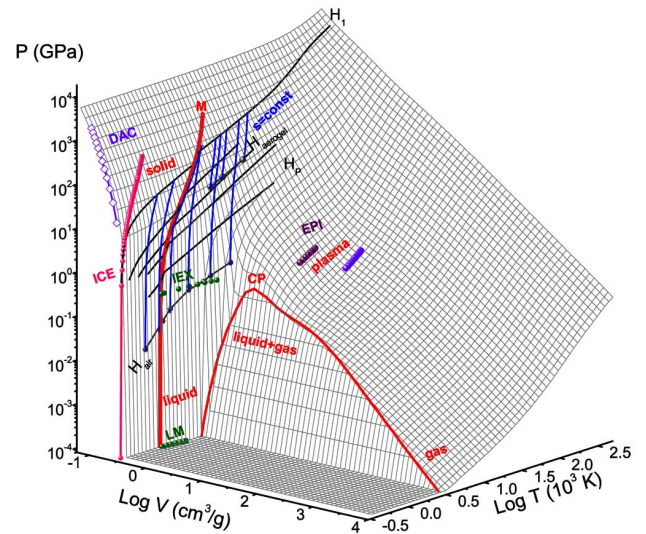
Fig. (2). Generalized 3D volume-temperature-pressure surface for aluminum. M-melting region; R-boundary of two-phase liquid-gas region with the critical point CP; H_1 and H_p -principal and porous Hugoniots; H_{air} and $H_{aerogel}$ - shock adiabats of air and aerogel; DAC-diamond-anvil-cells data; ICE-isentropic compression experiment; IEX-isobaric expansion data; S-release isentropes. Phase states of the metal are also shown.

Another important case of self-similar gas dynamic flow is the centered Riemann rarefaction wave. In experiments involving determination of isentropic expansion curves for a shock-compressed material, the states in the centered dumping wave are described by Riemann integrals [16]:

$$V_S = V_H + \int_{P_S}^{P_H} \left(\frac{dU}{dP}\right)^2 dP, \quad E_S = E_H - \int_{P_S}^{P_H} P\left(\frac{dU}{dP}\right)^2 dP, \quad (5)$$

where indexes S and H relate to isentrope and shock adiabat, correspondingly, and integrals are calculated along the measured isentrope $P = P_S(U)$.

These measurements of release isentropes of shocked materials are of especial importance. The adiabatic expansion of a substance, see curves s in Fig. (**2**), precompressed to megabar pressures by a shock wave, permits investigating an interesting plasma parameter domain located between a solid and a gas, including the metal-dielectric transition region and the high-temperature portion of the boiling curve of metals with their critical point [8, 43-45]. Since the metallic bond energy is rather high, the parameters of the critical points of metals are extremely high (4.5 kbar and 8000 K for aluminum, 15 kbar and 21000 K for tungsten [8]) and unattainable for static experimental techniques. That is why until recently the critical point characteristics were measured only for three of all metals, which account for ~80% of the elements of the Periodic Table [8]. On the other hand, because the critical temperatures of metals are high and are comparable to their ionization potentials, metals in a near-critical state vaporize directly to an ionized state and not to a gas, as is the case in the rest of the chemical elements. This circumstance may lead to exotic "plasma" phase transitions predicted for metallization by Ya. B. Zel'dovich and L. D. Landau [46] and other theorists for strongly compressed Coulomb systems (see Refs. [47-51] and references therein). Such results traverse states in the intermediate region between the solid state and gas, occupied by a hot dense metallic liquid and strongly coupled plasma [7, 8], which is a region poorly described by theory. Experimentally studied release isentropes have as initial high energy states solid, and melted, and compressed liquid metal. The range of thermodynamic parameters covered in the adiabatic expansion process for these states is extremely wide (Fig. **2**), covering five orders of magnitude in pressure and two orders of magnitude in density. It extends from a highly compressed metallic liquid, characterized by a disordered arrangement of ions and degenerate electrons, to a quasi-nonideal Boltzmann plasma and a rarefied metallic vapor. Upon expansion of the system, the degree of degeneracy of the electronic subsystem is decreased and a marked rearrangement of the energy spectrum of atoms and ions occurs. A partial recombination of the dense plasma also takes place. In the disordered electron system a "metal-insulator" transition takes place and a nonideal (with respect to different forms of interparticle interactions) plasma is formed in the vicinity of the liquid-vapor equilibrium curve and the critical point. Where isentropes enter the two-phase liquid-vapor region evaporation occurs; on the gas-side condensation occurs [7, 8, 20].

Note, that typical shock-wave measurements allow determination of only caloric properties of matter, viz. the dependence of the relative internal energy on pressure and volume as $E = E(P,V)$. The potential $E(P,V)$ is not complete in the thermodynamic sense and a knowledge of temperature T or entropy S is required for completing the thermodynamic equations and calculating first and second derivatives, such as the heat capacity, the sound velocity and others [8].

Only a few temperature measurements in shocked metals are available [52], as well as analogous measurements in release isentropic waves [20]. This information is of great importance in view of a limitation of purely theoretical calculation methods. From this point of view, thermodynamically complete measurements obtained with the use of the isobaric expansion (IEX) technique [53] are of a special significance. In this method metal is rapidly heated by a powerful pulsed current, then expands into an atmosphere of an inertial gas maintained at constant pressure. This data range in density form solid to the critical point and intersect, therefore, the release isentrope data for metals (see Fig. **2**). Data on slow electric discharge in metallic foil, "Enceinte à Plasma Isochore" (EPI) [54], are attributed to case of the isochoric heating and occupy the supercritical domain on the phase diagram.

The region between principal shock adiabat and isotherm can be accessed with use of the isentropic compression technique. This method allows one to obtain simultaneously high pressure and high densities in the material under study. In practice the sample is loaded by a magnetically driven impactor or by a sequence of reverberating shock waves in a multi-step compression process.

The final conclusion is that shock-wave techniques allow one to investigate material properties in very wide region of the phase diagram - from compressed solid to hot dense liquid, plasma, liquid-vapor, and quasi-gas states. Though the resulting high pressure, high and temperature information covers a broad range of the phase diagram, it has a heterogeneous character and, as a rule, is not complete from the thermodynamic point of view. Its generalization can be done only in the form of a thermodynamically complete EOS.

4. EOS: DEMANDS AND FORMULATION

The main goal of EOS development is its usage in gas dynamic codes. The experience of numerical modeling puts physical and mathematical demands and limitations to EOS.

This is wide range of applicability, i.e. EOS must describe thermodynamic properties in solid, liquid and plasma states. EOS also must be continuous and smooth in each phase. EOS for each phase must provide for mathematic conditions of resistance to compression (at $P(T = const) \to \infty$ one has $V \to 0$), stability of the heat conductivity ($C_V = (\partial E / \partial T)_V > 0$), existence of acoustic perturbations ($C_S = (\partial P / \partial \rho)_S^{1/2} > 0$) and stability of shock compression waves ($(\partial^2 P / \partial V^2)_T > 0$). The scalability means that new experimental or theoretical information can be easily implemented in EOS. Finally, the EOS part in gas dynamic calculations must be minimal. It is not simple to satisfy simultaneously all of these demands. This fact explains a great amount of EOS models.

EOS models are given by thermodynamically complete potentials. The free energy thermodynamic potential $F = E - TS$ is most suitable, its complete differential is

$$dF = -SdT - PdV \qquad (6)$$

The knowledge of $F(V,T)$ of the uniform system under condition of thermodynamic equilibrium allows one to determine partial derivatives which are used to obtain

measured thermodynamic functions and other potentials. Let us show it on example of the free energy:

$$P(V,T) = -\left(\frac{\partial F(V,T)}{\partial V}\right)_T = -F_V \tag{7}$$

$$S(V,T) = -\left(\frac{\partial F(V,T)}{\partial T}\right)_V = -F_T \tag{8}$$

$$C_V(V,T) = T\left(\frac{\partial S(V,T)}{\partial T}\right)_T = -T \times F_{TT} \tag{9}$$

$$C_P(V,T) = T\left(\frac{\partial S(V,T)}{\partial T}\right)_P = T\frac{\partial(S,P)}{\partial(T,V)}/\frac{\partial(T,P)}{\partial(T,V)} =$$

$$= T\left(\left(\frac{\partial S}{\partial T}\right)_V - \frac{\left(\frac{\partial P}{\partial T}\right)_V\left(\frac{\partial S}{\partial V}\right)_T}{\left(\frac{\partial P}{\partial V}\right)_T}\right) = T\left(-F_{TT} + \frac{F_{VT}^2}{F_{VV}}\right) \tag{10}$$

$$C_T^2(V,T) = -V^2\left(\frac{\partial P(V,T)}{\partial V}\right)_T = -V^2 F_{VV} \tag{11}$$

$$C_S^2(V,T) = -V^2\left(\frac{\partial P(V,T)}{\partial V}\right)_S = -V^2\frac{\partial(P,S)}{\partial(T,V)}/\frac{\partial(V,S)}{\partial(V,T)} =$$

$$= -V^2\left(\left(\frac{\partial P}{\partial V}\right)_T - \frac{\left(\frac{\partial S}{\partial V}\right)_T\left(\frac{\partial P}{\partial T}\right)_V}{\left(\frac{\partial S}{\partial T}\right)_V}\right) = -V^2\left(-F_{VV} + \frac{F_{VT}^2}{F_{TT}}\right) \tag{12}$$

Here in formulas (7), (8), (9),(10), (11), (12) P, S, C_V, C_P, C_T and C_S are pressure, entropy, heat capacities at constant volume and pressure, isothermal and isentropic sound velocities, correspondingly.

Considering a mixture of two phases 1 and 2of matter at given pressure and temperature also under condition of thermodynamic equilibrium with relative parts ξ and $(1-\xi)$, it is easy to obtain

$$V = \xi V_1 + (1-\xi)V_2 \tag{13}$$

$$S = \xi S_1 + (1-\xi)S_2 \tag{14}$$

$$\xi = \frac{V - V_1}{V_2 - V_1} = \frac{S - S_1}{S_2 - S_1} \tag{15}$$

Corresponding differentials are

$$dV = \xi dV_1 + (1-\xi)dV_2 + (V_1 - V_2)d\xi \tag{16}$$

$$dS = \xi dS_1 + (1-\xi)dS_2 + (S_1 - S_2)d\xi \tag{17}$$

$$d\xi = \frac{1}{V_2 - V_1}(\xi dV_1 + (1-\xi)dV_2) \tag{18}$$

The partial volume derivative is

$$F_{VV} = 0 \tag{19}$$

while the mixtured derivative is derived by Clausius-Clapeyron law

$$F_{VT} = \frac{dP}{dT} = \frac{S_2 - S_1}{V_2 - V1} \tag{20}$$

Using differentials of pressure

$$dP = \left(\frac{\partial P}{\partial V}\right)_T dV + \left(\frac{\partial P}{\partial T}\right)_V dT$$

and of entropy

$$dS = \left(\frac{\partial S}{\partial V}\right)_T dV + \left(\frac{\partial S}{\partial T}\right)_V dT$$

one can obtain

$$\frac{dV}{dT} = \frac{\frac{dP}{dT} - \left(\frac{\partial P}{\partial T}\right)_V}{\left(\frac{\partial P}{\partial V}\right)_T} \tag{21}$$

$$\frac{dS}{dT} = \left(\frac{\partial S}{\partial T}\right)_V + \left(\frac{\partial S}{\partial V}\right)_T\frac{dV}{dT} \tag{22}$$

Equations (17), (18), (20), (21), (22) allows one to determined the complete derivative of the mixture (here $A' = \frac{dA}{dT}$)

$$\frac{dS}{dT} = \xi S_1' + (1-\xi)S_2' - \frac{S_1 - S_2}{V_1 - V_2}(\xi V_1' + (1-\xi)V_2') =$$

$$= \xi\left(S_1' - V_1'\frac{dP}{dT}\right) + (1-\xi)\left(S_2' - V_2'\frac{dP}{dT}\right) \tag{23}$$

and the partial one

$$-F_{TT} = \left(\frac{\partial S}{\partial T}\right)_V = \xi\left[\left(\frac{\partial S}{\partial T}\right)_V + \left(\left(\frac{\partial P}{\partial T}\right)_V - \frac{dP}{dT}\right)\frac{\frac{dP}{dT} - \left(\frac{\partial P}{\partial T}\right)_V}{\left(\frac{\partial P}{\partial V}\right)_T}\right]_1 +$$

$$+ (1-\xi)\left[\left(\frac{\partial S}{\partial T}\right)_V + \left(\left(\frac{\partial P}{\partial T}\right)_V - \frac{dP}{dT}\right)\frac{\frac{dP}{dT} - \left(\frac{\partial P}{\partial T}\right)_V}{\left(\frac{\partial P}{\partial V}\right)_T}\right]_2 =$$

$$= \xi\left[-F_{TT} + \frac{\left(\frac{dP}{dT} + F_{VT}\right)^2}{F_{VV}}\right]_1 + (1-\xi)\left[-F_{TT} + \frac{\left(\frac{dP}{dT} + F_{VT}\right)^2}{F_{VV}}\right]_2 \tag{24}$$

where indexes relate to thermodynamic functions of phases 1 and 2.

Obviously, one can not use multi-phase EOS in gas dynamic codes directly. Indeed, thermodynamic derivatives are easily determined for the case of the uniform physical system, see Eqs. (9)-(12). These equations become much more complicated in the case of thermodynamically equilibrium two-phase system, see Eqs. (13)-(24). Note, that it is also necessary to know relative parts ξ and $(1-\xi)$ of

these phases. So the use of EOS in tabulated form is an efficient decision, which provides for good accuracy of EOS description and high performance of gas dynamic computations. The generation of tables using united EOS model [7, 25, 55, 56] guarantees the self consistency of thermodynamic functions.

As it seen from this consideration, in practice wide-range EOS means multi-phase EOS and, finally, tabulated EOS.

5. EOS OF TUNGSTEN

The semiempirical EOS model together with procedure of EOS constructing is described in details in [7, 24, 25]. Here we follow this methodology and present a detailed description of EOS for tungsten. All of the experimental and theoretical data have a given history of accuracy and reliability. The major problem in EOS construction is to provide for a self-consistent and non-contradictory description of the many kinds of available data. This section presents the calculation results of the thermodynamic properties and the phase diagram of tungsten in a manner used previously for aluminum. Again, the comparison with the experimental data and theoretical calculations is given for most significant at high pressures and temperatures information.

According to reference books [57, 58], tungsten is in *bcc* phase at room pressure, temperature. LMTO calculations at $T = 0$ K [59] predicts *bcc-hcp* and *hcp-fcc*-transitions at pressures of 12.5 and 14.4 Mbar, correspondingly, resulting from *sp-d*-delocalizing of electrons. DAC measurements at room temperature [60] show no phase transformations to 4.5 Mbar. Basing on this information, the EOS for tungsten was constructed for *bcc* phase.

The cold compression curve for tungsten is drawn in Fig. (**3**). The obtained cold curve, as it is seen from figure, agrees very good with semiempirical one [61] at moderate compression as well as with results of Thomas-Fermi theory [40] at extreme pressure to 100-fold compression. Calculated room-temperature isotherm also agrees with DAC measurements to 100 kbar [62].

The melting curve for tungsten was studied by optical method in one point at 50 kbar and 4050 ± 200 K with $dT / dP = 7.8$ K/kbar [58] and using laser-heated DAC to 900 kbar and 4050 ± 100 K [63]. Analogous slope of 4.4 K/kbar was obtained in IEX experiments [64]. The EOS provides for an intermediate value $dT / dP = 6$ K/kbar of initial slope of the melting curve. More accurate conclusions can be done only on the base of new more reliable experimental or theoretical data.

Tungsten is quite well studied in dynamic experiments. Shock compressibility of tungsten is investigated at megabar pressure with use of traditional explosive systems [19, 13, 65, 66] and two-stage light-gas gun [67, 68]. Results of shock compression of porous tungsten, obtained with the use of traditional plain and hemispherical explosive drivers to 3 Mbar [66, 69, 70-72], significantly expand investigated region of the phase diagram to lower densities. Nuclear
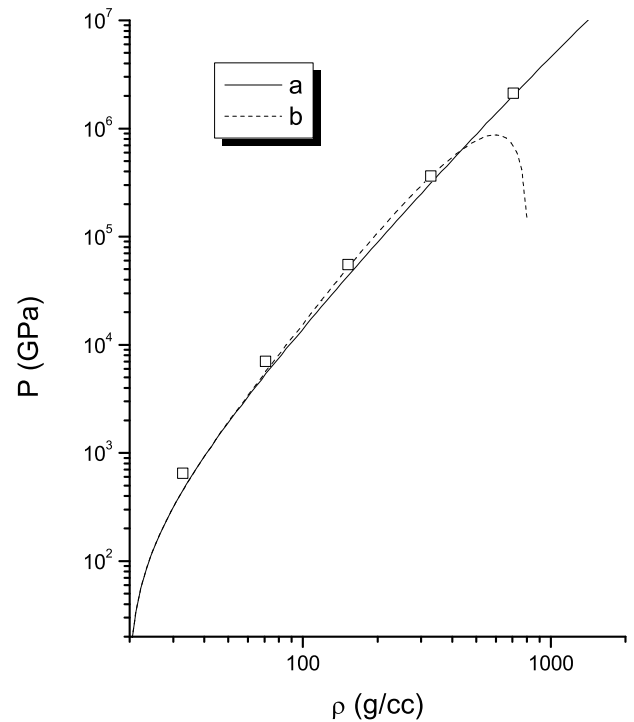
Fig. (3). Pressure-density diagram of tungsten at $T = 0$ K. Nomenclature: lines, a - EOS calculations, b-[61]; points - Thomas-Fermi calculations [40].
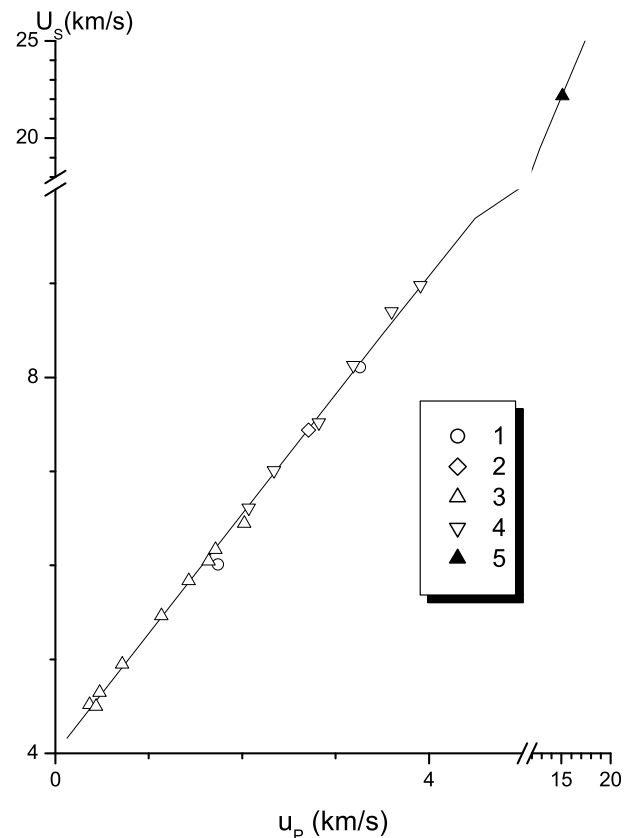
Fig. (4). Tungsten shock adiabat at high pressures. Nomenclature: line-EOS calculations; points-experiment, 1-[66], 2-[67], 3-[13], 4-[68], 5-[73].

impedance measurements are reported at 60 Mbar [73]. Analogous data on shock compression of porous ($m \simeq 3.05$) tungsten [74] at approximately normal density and pressure of $10 \div 20$ Mbar are of especial interest as they correspond to states of weakly degenerated electron gas with extremely high energy concentration of 2 MJ/g. The principal Hugoniot of solid tungsten at high pressure is compared against experimental data in kinematic shock velocity-mass velocity derivatives in Fig. (**4**). The phase diagram of tungsten at high pressure is presented in Fig. (**5**). The analysis of Figs. (**4**, **5**) proves the high fidelity of developed EOS in all investigated part of the phase diagram.
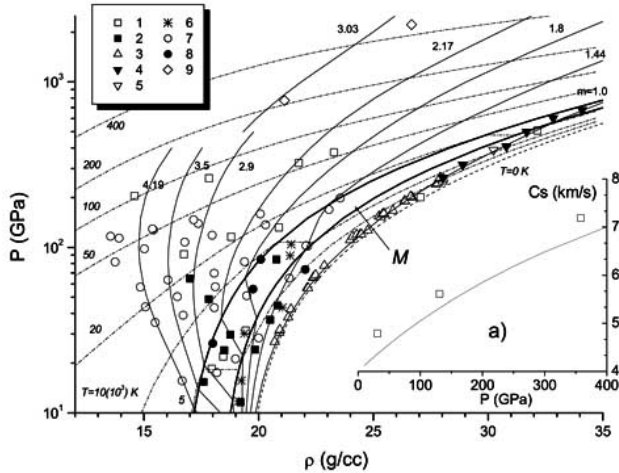
Fig. (5). Phase diagram of tungsten at high pressures. Nomenclature: lines-EOS calculations, T-isotherms, M-melting region, *m*-shock adiabats of porous samples ($m = \rho_0 / \rho_{00}$ -porosity); points-experimental data, 1-[66], 2-[71], 3-[13]; 4-[68], 5-[67], 6-[69], 7-[72], 8-[70], 9-[74]. a) Sound speed in shocked porous $m = 1.8$ tungsten. Line-EOS, points-experiment [66].

Release isentrope's measurements of shocked porous $m = 2.17$ tungsten [75] are of a special importance. Calculations prove that under conditions of fulfilled experiments initial states of shocked tungsten have high entropies, which leads to evaporating of metal in release waves, as it is shown in Fig. (**6**). The developed EOS describes these experimental points [75] with the accuracy of the experimental error ($\Delta U / U \leq 3\%$). This fact proves the reliability of calculation of thermodynamic properties of liquid tungsten and, intermediately, the position of evaporating region at high pressure. Unfortunately, the character of experimental $P - U$-dependencies does not fix a clean break, which can attribute uniquely the boundary position of two-phase liquid-gas mixture with respect to pressure.

IEX data are available for tungsten in region of lower densities [76-78]. The comparison with these data is given in Fig. (**7**). It is well seen that IEX points occur inside two-phase liquid-gas domain, which can be attributed to non-equilibrium conditions of mentioned experiments. One should note, that the evaluation of the critical point [79], based on [76], leads to an assumption of strong convexity on the evaporating curve. Analogous more recent evaluation of
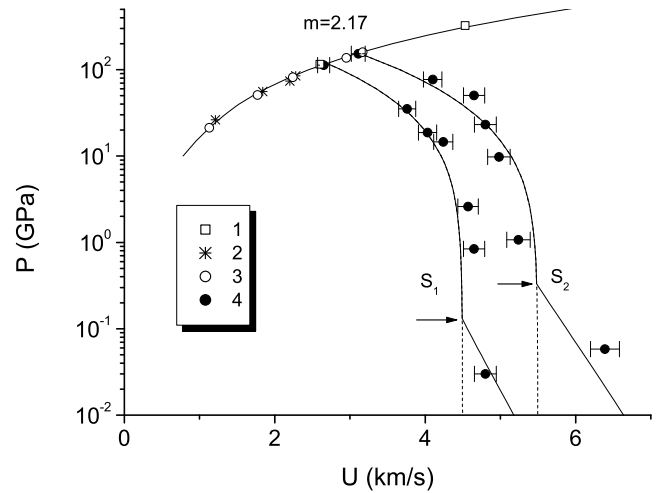
Fig. (6). Release isentropes of tungsten. Nomenclature: lines-EOS calculations, *m*-shock adiabat of porous tungsten, s_i-release isentropes, arrows indicate entrance in evaporating region; points-experiment, 1-[66], 2-[70], 3-[72], 4-[75].
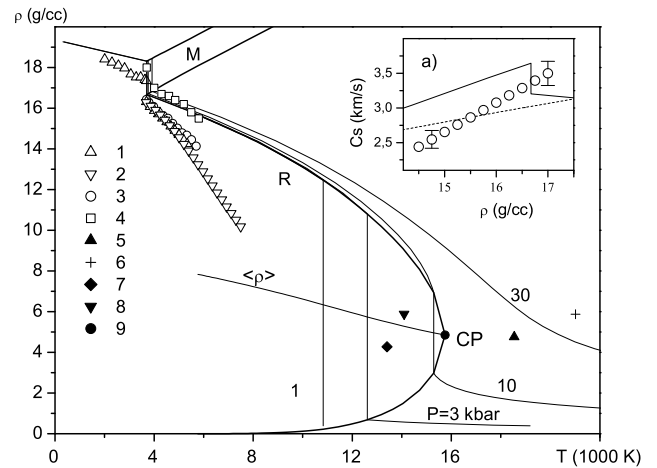
Fig. (7). Phase diagram of tungsten at lower densities. Nomenclature: lines-EOS calculations, M-melting region, R-liquidgas region with the critical point CP, P-isobars; points-experiment, 1-[77], 2-[76], 3-[78], 4-[81], and evaluations of the critical points, 5-[84], 6-[8], 7-[80], 8-[79], 9-this work. **a)** Sound speed in liquid tungsten, line - EOS, points - experiment [78].

these authors [80], based on spinodal EOS, reached in heating process, also does not agree in this sense to their experiments [76]. Most recent paper [81] on this problem fixes good effects of melting and evaporating while the value of heat capacity for liquid metal ~0.27 J/(gK) is close to results of work [78]. This paper is the only one which does not disagree with available evaluations of the critical point of tungsten, see Fig. (**7**). The gas-thermal method [82] was used to heat tungsten along boiling curve. The evaluation of critical point $P_c = 5.8 \pm 0.5$ kbar, $T_c = 13660 \pm 800$ K corresponds to abrupt change of the optic properties under conditions of this experiment. The developed EOS for tungsten provides for alternative description of two-phase liquid-gas region and position of the critical point as $P_c = 11.80$ kbar, $T_c = 15750$ K, $V_c = 0.206$ cc/g, $S_c = 0.837$ J/(gK) against available evaluations. The calculated value of

evaporating temperature at room pressure $T_v = 5766$ K agrees with given in reference book [83] value 5953 K, which is known with an accuracy of 10%.

6. CONCLUSION

Experiments in physics of high pressures has made it possible to obtain in laboratory conditions states of matter with extremely high energy densities typical for of the first seconds of the expansion of the Universe after the Big Bang and the states typical for such astrophysical objects as stars, giant planets, and exoplanets.

The information gained in dynamic experiments substantially broadens our basic notions about the physical proper ties of matter in a vast domain of the phase diagram up to ultrahigh pressures, which exceed the atmospheric pressure by 10 orders of magnitude, and to temperatures exceeding the human body temperature by 7 orders of magnitude.

Today shock-wave methods provide for most important from practical point of view information for developing wide-range EOS. Most powerful EOS are based on correct theoretical models and describe with high accuracy and reliability a broad range of the phase diagram, from the high-pressure shocked metal to more dense states in reflected shock waves and to regions of the phase diagram with much lower densities accessed in the process of the adiabatic expansion of shocked metal. The high accuracy suits EOS to be applied in advanced numerical modeling for solving numerous problems in the physics of high energy densities.

REFERENCES

[1]   Al'tshuler LV. Use of shock waves in physics of high pressure. Sov Phys Usp 1965; 8: 52-91.

[2]   Bushman AV, Fortov VE. Model equations of state. Sov Phys Usp 1983; 26: 465-96.

[3]   Elieser S, Ghatak AK, Hora H. An introduction to equations of state: theory and applications. Cambridge: Cambridge University Press 1986.

[4]   Ross M. Matter under extreme conditions of temperature and pressure. Rep Progr Phys 1985; 48: 1-52.

[5]   Chisolm ED, Crockett SD, Wallace DC. Test of a theoretical equation of state for elemental solids and liquids. Phys Rev B 2003; 68: 04103.

[6]   Bushman AV, Lomonosov IV, Fortov VE. Equations of State for Metals at High Energy Density [in Russian]. Chernogolovka: Inst Chem Phys Chernogolovka RAS 1992.

[7]   Bushman AV, Kanel GI, Ni AL, Fortov VE. Thermophysics and dynamics of intense pulse loadings. London: Taylor&Fransis 1993.

[8]   Fortov VE, Khrapak AG, Yakubov IT. Physics of nonideal plasmas. Oxford: Clarendon Press 2006.

[9]   Grüneisen E. Theorie des festen zustandes einatomiger elemente. Ann Phys 1912: 39: 257-306.

[10]   Birch F. On the possibility of large changes in the Earth's volume. Phys Earth Planet Interiors 1968; 1: 141-147.

[11]   Carnahan NF, Starling KE. Equation of state for nonattracting rigid spheres. J Chem Phys 1969; 51: 635-6.

[12]   Van Thiel M, Ed. Compendium of shock wave data. Report UCRL-50108, Lawrence Livermore Lab., Livermore 1977.

[13]   Marsh SP, Ed. LASL Shock Hugoniot Data. Berkeley: University of California Press 1980.

[14]   Zhernokletov MV, Zubarev VN, Trunin RF, Fortov VE. Experimental data on shock compressibility and adiabatic expansion of condensed matter at high energy density Chernogolovka, Moscow Oblast: Institute of Chemical Physics in Chernoglovka, Russian Academy of Sciences 1996.

[15]   Trunin RF, Gudarenko LF, Zhernokletov MV, Simakov GV. Experimental data on shock compression and adiabatic expansion of condensed matter [in Russian]. Sarov: RFNC-VNIIEF 2001.

[16]   Zeldovich YB, Raizer YP. Physics of shock waves and high-temperature hydrodynamic phenomena. New York: Academic Press 1966.

[17]   Ashcroft NW, Mermin ND. Solid State Physics. New York: Holt, Rinehart and Winston 1976.

[18]   Barker JA and Henderson D. What is liquid? understanding the states of matter. Rev Mod Phys 1976; 48: 587-671.

[19]   McQueen RG, Marsh SP, Taylor JW, Fritz JN, Carter WJ. The equation of state of solids from shock wave studies. In: Kinslow R, Ed. High velocity impact phenomena. London: Academic Press 1970; pp. 293-417. Appendices on pp. 515-68.

[20]   Avrorin EN, Vodolaga BK, Simonenko VA, Fortov VE. Powerful shock waves and extreme states of matter [in Russian]. Moskva: IVTAN 1990.

[21]   Duvall GE, Graham RA. Phase transitions under shock-wave loading. Rev Mod Phys 1977; 49: 523-79.

[22]   Fortov VE. Extreme states of matter on earth and in space. Phys Usp 2009; 52(6): 615-48.

[23]   Fortov VE, Lomonosov IV. Shock waves and equations of state of matter. Shock Waves 2009; doi: 10.1007/s00193-009-0224-8.

[24]   Fortov VE, Lomonosov IV. Thermodynamics of extreme states of matter. Pure Appl Chem 1997; 69(4): 893-904.

[25]   Lomonosov IV. Multi-phase equation of state for aluminum. Laser Part Beams 2007; 25: 567-84.

[26]   Avrorin EN, Vodolaga BK, Simonenko VA, Fortov VE. Intense shock waves and extreme states of matter. Phys Usp 1993; 36: 337-64.

[27]   Hogan WJ, Ed. Energy from inertial fusion (sti/pub/944), Technical report, International Atomic Energy Agency, Vienna, Austria 1995.

[28]   Altshuler LV, Trunin RF, Krupnikov KK, Panov NV. Explosive laboratory devices for shock wave compression studies. Phys Usp 1996; 39(5): 539-44.

[29]   Kanel GI, Razorenov SV, Utkin AV, Fortov VE. Shock-wave phenomena in condensed media. Moscow: Yanus-K 1996.

[30]   Altshuler LV, Trunin RF, Urlin VD, Fortov VE, Funtikov AI. Development of dynamic high-pressure techniques in russia. Phys Usp 1999; 42(3): 261-80.

[31]   Fortov VE, Khrapak AG, Khrapak SA, Molotkov VI, Petrov OF. Dusty plasmas. Phys Usp 2004; 47: 447-92.

[32]   Walsh JM, Rice MH, McQueen RG, Yarger FL. Shock-wave compressions of twenty-seven metals equations of state of metals. Phys Rev 1957; 108: 196-221.

[33]   Al'tshuler LV, Krupnikov KK, Ledenev BN, Zhuchikhin VI, Brazhnik MI. Dynamical compressibility and equation of state for iron under high pressure. Sov Phys - JETP 1958; 7: 606-13.

[34]   Al'tshuler LV, Krupnikov KK, Brazhnik MI. Dynamical compressibility of metals under pressure from 400000 to 4 million atmospheres. Sov Phys - JETP 1958; 34: 614-8.

[35]   Kormer SB, Funtikov AI, Urlin VD, Kolesnikova AN. Dynamical compression of porous metals and the equation of state with variable specific heat at high temperatures. Sov Phys - JETP 1962; 15: 477-88.

[36]   Al'tshuler LV, Bakanova AA, Dudoladov IP, Dynin EA, Trunin RF, Chekin BS. Shock adiabatic curves for metals. new data, statistical analysis and general laws. J Appl Mech Tech Phys 1981; 22: 145-69.

[37]   Al'tshuler LV, Moiseev BN, Popov LV, Simakov GV, Trunin RF. Relative compressibility of iron and lead at pressures of 31 to 34 Mbar. Sov Phys - JETP 1968; 27: 420-2.

[38] Trunin RF, Podurets MA, Moiseev BN, Simakov GV, Popov LV. Relative compressibility of copper, cadmium and lead at high pressures. Sov Phys - JETP 1969; 29: 630-1.

[39] Vladimirov AS, Voloshin NP, Nogin VN, Petrovtsev AV, Simonenko VA. Shock compressibility of aluminum at p ˛ 1 Gbar. Sov Phys - JETP Lett 1984; 39: 85-8.

[40] Kalitkin NN, Kuzmina LV. Reprint [in Russian] N35, Inst Prikl Matem Akad Nauk SSSR, Moskva 1975.

[41] Trunin RF, Podurets MA, Popov LV, *et al.* Measurement of the iron compressibility at pressures of 5.5 TPa. Sov Phys - JETP 1992; 75: 777-80.

[42] Trunin RF, Podurets MA, Moiseev BN, Simakov GV, Sevastyanov AG. Determination of the shock compressibility of iron at pressures up to 10 TPa (100 Mbar). Sov Phys - JETP 1993; 76: 1095-8.

[43] Fortov VE, Al'tshuler LV, Trunin RF, Funtikov AI. Shock waves and extreme states of matter: high-pressure shock compression of solids VII. New York: Springer 2004.

[44] Al'tshuler LV, Bakanova AA, Bushman AV, Dudoladov IP, Zubarev VN. Evaporation of shock-compressed lead in release waves. Sov Phys - JETP 1977; 46(5): 980-3.

[45] Al'tshuler LV, Bushman AV, Zhernokletov MV, Zubarev VN, Leont'ev AA, Fortov VE. Unload isentropes and equation of state of metals at high energy densities. Sov Phys - JETP 1980; 51: 588-91.

[46] Zel'dovich YB, Landau LD. Relation of the liquid to gaseous state at metals. Zh Eksp Teor Fiz 1944; 14: 32.

[47] Wigner E. On the interaction of electrons in metals. Phys Rev 1934; 46: 1002.

[48] Ebeling V, Forster A, Fortov VE, Gryaznov VK, Polishchuk AY. Thermophysical properties of hot dense plasmas. Stuttgart: B.G. Teubner Verlagsgesellschaft 1991.

[49] Norman GE, Starostin AN. Thermodynamics of a strongly nonideal plasma. High Temp 1970; 8: 381.

[50] Saumon D, Chabrier G. Fluid hydrogen at high density: the plasma phase transition. Phys Rev Lett 1988; 62: 2397.

[51] Filinov VS, Fortov VE, Bonitz M, Levashov PR. Phase transition in strongly degenerate hydrogen plasma. JETP Lett 2001; 74: 384-7.

[52] Yoo CS, Holmes NC, Ross M, Webb DJ, Pike C. Shock temperature and melting of iron at Earth core conditions. Phys Rev Lett 1993; 70(25): 3931-4.

[53] Gathers GR. Dynamic methods for investigating thermophysical properties of matter at very high temperatures and pressures. Rep Prog Phys 1986; 49: 341-396.

[54] Renaudin P, Blancard C, Clerouin J, Faussurier G, Noiret P, Recoules V. Aluminum equation-of-state data in the warm dense matter regime. Phys Rev Lett 2003; 91(7): 075002.

[55] Kerley GI. Theoretical equation of state for aluminum. Int J Impact Eng 1987; 5: 441-449.

[56] Young DA, Corey EM. A new global equation of state model for hot, dense matter. J Appl Phys 1995; 78(6): 3748-55.

[57] Young DA. Phase diagrams of the elements. Berkely: University of California Press 1991.

[58] Tonkov EY, Ponyatovsky EG. Phase transformations of elements under high pressure. Washington DC: CRC Press 2004.

[59] Moriarty J. Ultrahigh-pressure structural phase transitions in Cr, Mo and W. Phys Rev B 1992; 45: 2004-14.

[60] Ruoff AL, Luo H, Vanderborgh C, Vohra YK. Generating nearearth-core pressures with type-iia diamonds. Appl Phys Lett 1991; 59: 2681-2.

[61] Kormer SB, Urlin VD, Popova LT. Interpolation equation of state and its application to description of experimental data on shock compression of metals [in Russian]. Fizika Tverdogo Tela 1961; 3: 2131-40.

[62] Ming LC, Manghnani MH. Isothermal compression of bcc transition metals to 100 kbar. J Appl Phys 1978; 48: 208-12.

[63] Errandonea D, Schwager B, Ditz R, Gessmann C, Boehler R, Ross M. Test of a theoretical equation of state for elemental solids and liquids. Phys Rev B 2001; 63: 132104.

[64] Shaner JW, Gathers GR, Minichino. A new apparatus for thermophysical measure-ments above 2500 K. High Temp - High Press 1976; 8: 425-9.

[65] McQueen RG, Marsh SP. Equation of state for nineteen metallic elements. J Appl Phys 1960; 31: 1253-69.

[66] Krupnikov KK, Brazhnik MI, Krupnikova VP. Shock compression of porous tungsten. Sov Phys - JETP 1962; 15: 470-6.

[67] Jones AH, Isbell WH, Maiden CJ. Measurements of the very highpressure properties of materials using a light-gas gun. J Appl Phys 1966; 37: 3493-9.

[68] Hixson RS, Fritz JN. Shock compression of tungsten and molybdenum. J Appl Phys 1992; 71: 1791-28.

[69] Boade RR. Dynamic compression of porous tungsten. J Appl Phys 1969; 40: 3781-92.

[70] Alekseev YuL, Ratnikov BP, Rybakov AP. Shock adiabats of porous metals [in Russian]. Zh Prikl Mekh Tekhn Fiz 1971; 2: 101-6.

[71] Bakanova AA, Dudoladov IP, Sutulov Yu N. Shock compressibility of porous tungsten, molybdenum, copper, and and aluminum in low pressure range. J Appl Mech Tech Phys 1974; 15: 241.

[72] Trunin RF, Simakov GV, Sutulov YuN, Medvedev AB, Rogozkin BD, and Fedorov YuE. Compression of porous metals in shock waves. Sov Phys - JETP 1989; 69: 580-831.

[73] Ragan CE. Shock compression measurements at 1 to 7 TPa - Phys Rev Ser A 1982; 25: 3360-75.

[74] Trunin RF, Medvedev AB, Funtikov AI, Podurets MA, Simakov GV, Sevast'yanov AG. Shock compression of porous iron, copper, and tungsten and their equation of state in terapascal pressure range. Sov Phys - JETP 1989; 68: 356-61.

[75] Gudarenko LF, Gushchina ON, Zhernokletov MV, Medvedev AB, Simakov GV. Shock compression and isentropic expansion of tungsten, nickel and tin porous samples [in Russian]. Teplo - Vys Temp 2000; 38(3): 437-44.

[76] Seydel U, Kitzel W. Thermal volume expansion of liquid Ti, V, Mo, Pd. J Phys: F Metal Phys 1979; 9(9): L153-L160.

[77] Berthault A, Arles L, Matricon J. High-pressure, high-temperature thermophysical measurements on tantalum and tungsten. Int J Thermophys 1986; 7(1): 169-79.

[78] Hixson RS, Winkler MA. Thermophysical properties of solid and liquid tungsten. Int J Thermophys 1990; 11(4): 709-18.

[79] Seydel U, Bauhof H, Fucke W, Wadle H. Thermophysical data for various transition metals at high temperatures obtained by a submicrosecond-pulse-heating method. High Temp - High Press 1979; 11(6): 635-42.

[80] FuckeW, Seydel U. Improved experimental determination of critical point data for tungsten. High Temp - High Press 1980; 12(4): 419-32.

[81] Koval SV, Kuskova NI, Tkachenko SI. Investigation of currents explosion mechanism and thermophysical properties of liquid metals [in Russian]. Teplo Vys Temp 1997; 35(6): 876-9.

[82] Ternovoi V, Filimonov A, Fortov V, Gordon Yu, Nikolaev D, Pyalling A. Liquid|vapor phase boundaries determination by dynamic experimental method. Bull Am Phys Soc 1999; 44(2): 95.

[83] Kikoin IK. Tables of physical constatnts. Reference book [in Russian]. Moscow: Energoatomizdat 1976.

[84] Young DA, Alder BJ. Critical points of metals from the van der Waals model. Phys Rev A 1971; 3: 364-71.